Earth and Planetary Science Letters 492 (2018) 22–34

Contents lists available at ScienceDirect

Earth and Planetary Science Letters

www.elsevier.com/locate/epsl

On the origin of the marine zinc–silicon correlation

Gregory F. de Souza [a,*], Samar P. Khatiwala [b], Mathis P. Hain [c], Susan H. Little [d], Derek Vance [a]

[a] ETH Zurich, Institute of Geochemistry and Petrology, Clausiusstrasse 25, 8092 Zurich, Switzerland
[b] Department of Earth Sciences, University of Oxford, South Parks Road, Oxford OX1 3AN, UK
[c] National Oceanography Centre, University of Southampton, Southampton SO14 3ZH, UK
[d] Department of Earth Science and Engineering, Imperial College London, London SW7 2BP, UK

ARTICLE INFO

Article history:
Received 18 September 2017
Received in revised form 23 March 2018
Accepted 25 March 2018
Available online 10 April 2018
Editor: M. Frank

Keywords:
ocean biogeochemistry
Southern Ocean
diatoms
GEOTRACES

ABSTRACT

The close linear correlation between the distributions of dissolved zinc (Zn) and silicon (Si) in seawater has puzzled chemical oceanographers since its discovery almost forty years ago, due to the apparent lack of a mechanism for coupling these two nutrient elements. Recent research has shown that such a correlation can be produced in an ocean model without any explicit coupling between Zn and Si, via the export of Zn-rich biogenic particles in the Southern Ocean, consistent with the observation of elevated Zn quotas in Southern Ocean diatoms. Here, we investigate the physical and biological mechanisms by which Southern Ocean uptake and export control the large-scale marine Zn distribution, using suites of sensitivity simulations in an ocean general circulation model (OGCM) and a box-model ensemble. These simulations focus on the sensitivity of the Zn distribution to the stoichiometry of Zn uptake relative to phosphate (PO_4), drawing directly on observations in culture. Our analysis reveals that OGCM model variants that produce a well-defined step between relatively constant, high Zn:PO_4 uptake ratios in the Southern Ocean and low Zn:PO_4 ratios at lower latitudes fare best in reproducing the marine Zn–Si correlation at both the global and the regional Southern Ocean scale, suggesting the presence of distinct Zn-biogeochemical regimes in the high- and low-latitude oceans that may relate to differences in physiology, ecology or (micro-)nutrient status. Furthermore, a study of the systematics of both the box model and the OGCM reveals that regional Southern Ocean Zn uptake exerts control over the global Zn distribution via its modulation of the biogeochemical characteristics of the surface Southern Ocean. Specifically, model variants with elevated Southern Ocean Zn:PO_4 uptake ratios produce near-complete Zn depletion in the Si-poor surface Subantarctic Zone, where upper-ocean water masses with key roles in the global oceanic circulation are formed. By setting the main preformed covariation trend within the ocean interior, the subduction of these Zn- and Si-poor water masses produces a close correlation between the Zn and Si distributions that is barely altered by their differential remineralisation during low-latitude cycling. We speculate that analogous processes in the high-latitude oceans may operate for other trace metal micronutrients as well, splitting the ocean into two fundamentally different biogeochemical, and thus biogeographic, regimes.

1. Introduction

As a phytoplankton micronutrient, zinc is a highly versatile element, playing a role as co-factor in metalloenzymes required for biological tasks as varied as carbon fixation (Price and Badger, 1989), gene expression (Twining and Baines, 2013) and the uptake of key macronutrients such as phosphorus and, potentially, silicon (Rueter and Morel, 1981; Sherbakova et al., 2005; Morel et al., 2014). Indeed, the physiological importance of zinc rivals that of iron (Fe), with more Zn-bearing metalloenzymes known than Fe-bearing ones (Morel et al., 2014). And yet the marine Zn cycle has received limited attention, most likely the result of a long-standing lack of observational data on the abundance of dissolved Zn in the sea. Within the last five years, the efforts of the GEOTRACES programme have produced an order-of-magnitude change in the volume of marine Zn abundance data (Mawji et al., 2015).

In a recent companion study, Vance et al. (2017) took advantage of this step-change in data availability to study the mechanisms

* Corresponding author at: ETH Zurich, Institute of Geochemistry and Petrology, NW C83.1, Clausiusstrasse 25, 8092 Zurich, Switzerland.
E-mail address: desouza@erdw.ethz.ch (G.F. de Souza).

https://doi.org/10.1016/j.epsl.2018.03.050
0012-821X/

responsible for producing the observed oceanic Zn distribution. It has been known since the very first reliable analyses of oceanic Zn concentration (Bruland, 1980) that the Zn distribution mimics that of dissolved silicon, a macronutrient that is obligatorily required, and dominantly cycled, by the siliceous phytoplankton known as diatoms. The reasons for the very close, near-linear correlation (Fig. S3) between these two elements in the ocean has, however, remained unclear for over three decades. A direct mechanism, such as the incorporation of Zn into the siliceous frustules of diatoms (Broecker and Peng, 1982), is not permitted by the observation that the Zn content of diatom frustules is orders of magnitude too small to produce the observed correlation between Zn and Si (Ellwood and Hunter, 2000). Furthermore, recent cellular-level elemental mapping has revealed that Zn is mostly associated with the organic matter of diatoms (Twining et al., 2004), consistent with its important physiological role, and that cellular Zn is remineralised from sinking diatom detritus at shallow depths together with phosphorus, not at the greater depths at which siliceous hard parts dissolve (Twining et al., 2014). Thus, the simple correlation between the marine distributions of Zn and Si at the global scale appears at odds with their contrasting biochemical roles and marine biogeochemical behaviour.

Vance et al. (2017) resolved this apparent paradox by drawing on the observation that diatoms in the Southern Ocean have cellular Zn quotas 3–15× higher than those of low-latitude phytoplankton (Twining and Baines, 2013), a finding that is complemented by the observed stripping of Zn from Southern Ocean surface waters (Ellwood, 2008; Zhao et al., 2014). In analogy to the well-established control on the marine Si distribution by the export of Si-rich material from the surface Southern Ocean (Sarmiento et al., 2007), Vance et al. (2017) proposed that strong Zn drawdown by Southern Ocean diatoms with high Zn quotas is the main control on the global Zn distribution. Their ocean general circulation model (OGCM) results supported this hypothesis by reproducing the observed Zn–Si correlation when Southern Ocean Zn uptake was high, even in the absence of any explicit coupling between the cycles of these two elements.

The aim of this study is to identify the mechanisms by which this emergent large-scale Zn–Si coupling comes about. Our interest lies in understanding the series of interacting biological and physical processes that allows Zn uptake in the remote Southern Ocean to influence the global Zn distribution. We do this within the context of ocean biogeochemical models in which the cycling of Zn is explicitly tied to that of phosphorus (P), and go beyond the modelling work of Vance et al. (2017) by implementing a swathe of 24 OGCM sensitivity simulations as well as a 10,000-member box-model ensemble. Together, these simulations reveal that Southern Ocean Zn uptake exerts global control on the marine Zn distribution via its influence on the Zn status of the Subantarctic Zone (SAZ): sustained and elevated high-latitude Zn uptake leads to Zn-depletion in the Si-poor SAZ, producing a low-Zn, low-Si signal that is transported globally from this region by the subduction of the upper-ocean water masses Subantarctic Mode Water (SAMW) and Antarctic Intermediate Water (AAIW). The systematics of the models further suggest that this coupled biological–physical mechanism may apply more generally to other biologically-cycled elements in the sea.

2. Methods

2.1. Conceptual approach

We wish to assess the mechanisms by which a correlation between the marine distributions of Zn and Si may come about even in the absence of any explicit coupling between them. We do this in the context of ocean models, described in more detail below,

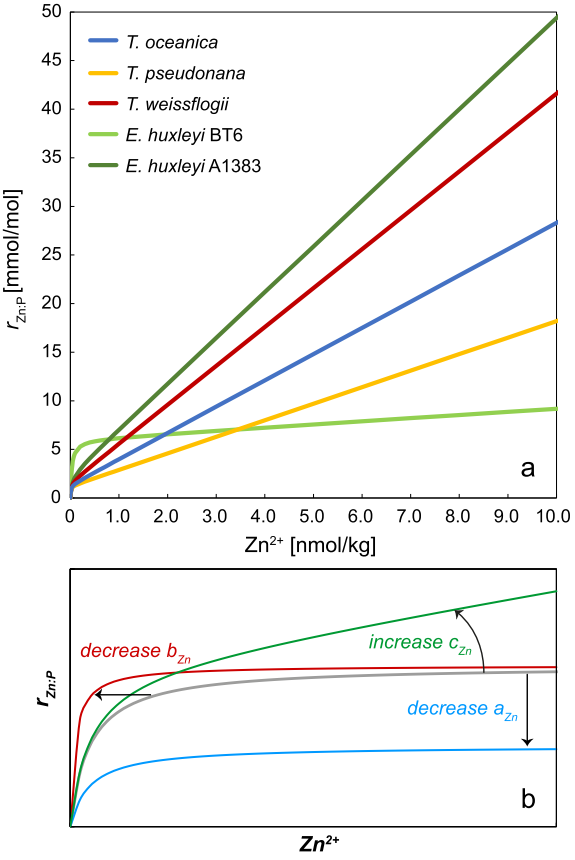

Fig. 1. Stoichiometry of simulated uptake. Panel *a* shows the dependence of the Zn:P uptake ratio $r_{Zn:P}$ on the ambient concentration of Zn^{2+} observed in culture experiments by Sunda and Huntsman (1992). Data in Sunda and Huntsman (given as Zn:C ratios) have been converted to Zn:P using the Redfield C:P ratio of 106 mol/mol. Panel *b* schematically illustrates the influence of the parameters a_{Zn}, b_{Zn} and c_{Zn} in Eqn. (1) on the shape of this dependency. (For interpretation of the colours in the figure(s), the reader is referred to the web version of this article.)

that simulate the marine biogeochemical cycles of P, Zn and Si. In formulating the biogeochemical model, we were guided by the observations and constraints discussed in Section 1. Thus, our model explicitly couples the cycling of Zn to that of P, reflecting observations of Zn uptake in culture, our understanding of the physiological role of Zn as a micronutrient, and direct observation of the Zn distribution within phytoplankton cells (Sunda and Hunstman, 1992; Twining et al., 2004; Twining and Baines, 2013). The simulated surface–ocean uptake of Zn is directly tied to that of PO_4 by a stoichiometric parameter $r_{Zn:P}$, which is the key variable in our sensitivity analysis (see Section 2.2). Additionally, once exported from the surface ocean by sinking particles, Zn is remineralised over the same short length-scale as P, as indicated by observations of sinking diatoms (Twining et al., 2014). In contrast, simulated Si uptake is entirely independent of PO_4 uptake, and the length-scale of opal dissolution is greater than that of Zn or P remineralisation, rendering its cycling entirely biogeochemically independent.

2.2. Stoichiometry of simulated Zn uptake

The control parameter in our suite of sensitivity simulations is the stoichiometric parameter $r_{Zn:P}$, which links the uptake of Zn to the simulated PO_4 uptake. Our parameterisation of $r_{Zn:P}$ is based on results from laboratory cultures of three diatom species and two clones of the prymnesiophyte *E. huxleyi* by Sunda and Huntsman (1992). They observed that the Zn:C (and, by extension, Zn:P) ratio of phytoplankton uptake is a non-linear function of the Zn^{2+}

concentration of the growth medium, described by an equation of the form:

$$r_{Zn:P} = \underbrace{\frac{a_{Zn} \cdot Zn^{2+}}{b_{Zn} + Zn^{2+}}}_{(I)} + \underbrace{c_{Zn} \cdot Zn^{2+}}_{(II)} \quad (1)$$

This equation is the linear superposition of a saturating Michaelis–Menten term (I) and a non-saturating linear term (II), which is illustrated by the shape of curves fit to the culture data of Sunda and Huntsman (1992) in Fig. 1a. The species Zn^{2+} represents free aqueous Zn in solution, i.e. Zn that is neither inorganically nor organically complexed. Considering only organic speciation, the concentration of Zn^{2+} is governed by the total concentration of dissolved Zn on the one hand, and the concentration (and binding characteristics) of the chelating organic ligand on the other. We assume a globally constant ligand concentration of 1.2 nM, which allows us to circumvent the explicit simulation of Zn complexation chemistry (see Supplementary Information). The assumption of constant ligand concentrations is doubtless an oversimplification, but the sparse observational dataset shows only limited variability (~0.6–2.4 nM) with no systematic variation (Donat and Bruland, 1990; Bruland, 1989; Ellwood and van den Berg, 2000; Ellwood, 2004; Lohan et al., 2005; Baars and Croot, 2011). This variability in ligand concentrations is small relative to the orders-of-magnitude variability of dissolved Zn in the ocean. Sensitivity simulations documented in the Supplementary Information (Fig. S11) show that the choice of ligand concentration does not affect the systematics of our results, and thus has no influence on our interpretation.

Parameters a_{Zn}, b_{Zn} and c_{Zn} of Eqn. (1) control different aspects of the dependency of $r_{Zn:P}$ on Zn^{2+}, as illustrated schematically in Fig. 1b. Parameter a_{Zn} determines the maximum asymptotic Zn:PO_4 ratio of uptake when the Michaelis–Menten term of Eqn. (1) saturates, whilst b_{Zn} controls the sensitivity of $r_{Zn:P}$ to low Zn^{2+} concentrations. The linear parameter c_{Zn}, on the other hand, determines the extent to which high Zn^{2+} affects $r_{Zn:P}$ beyond the asymptotic Zn:PO_4 ratio determined by a_{Zn}. In this paper, we present the results of 24 OGCM sensitivity simulations in which the values of these parameters are varied (Table 1). In our base suite of simulations (G1–G11), also presented in Vance et al. (2017), the values of a_{Zn}, b_{Zn} and c_{Zn} are set so as to reproduce the dependence of $r_{Zn:P}$ on Zn^{2+} in the culture data of Sunda and Huntsman (1992), i.e. the curves shown in Fig. 1a (G7–G11), or an approximation thereof in which $r_{Zn:P}$ is a linear function of Zn concentration (G1–G6; see Supplementary Information). In a further 13 simulations (G12–G24), parameters a_{Zn}, b_{Zn} and c_{Zn} are separately varied within the bounds of the culture data, in order to explore their individual influence on the spatial distribution of $r_{Zn:P}$ and the marine Zn distribution.

2.3. Model framework

OGCM simulations were run on the high-performance cluster *Euler* at ETH Zurich using the transport-matrix method (TMM) of Khatiwala et al. (2005), which allows efficient offline simulation of passive tracers. Here, we use transport matrices derived from MITgcm-2.8, a coarse-resolution version of MITgcm (Marshall et al., 1997) with 2.8° × 2.8° lateral resolution and 15 vertical levels (see Supplementary Information). Simulations were carried out with annual-mean circulation fields derived from the equilibrium state of the model, and thus do not include seasonal variability.

Our biogeochemical model of P, Si and Zn cycling is based on the formulation developed for the OCMIP-2 project (Najjar et al., 2007), with simulated uptake of PO_4 and Si in the surface ocean driven by restoring their concentrations towards observations in World Ocean Atlas 2013 (Garcia et al., 2013; see Supplementary Information). As discussed in Section 2.2, Zn uptake is directly tied to that of PO_4 by the stoichiometric parameter $r_{Zn:P}$. Both Zn and P in the particulate export flux are remineralised following a power-law depth-dependency with an exponent of −0.858 (Martin et al., 1987; Berelson, 2001), whereas regeneration of Si follows an exponential dependency with a length-scale of 1000 m (de Souza et al., 2014). Based on World Ocean Atlas 2013 and literature data, the mean ocean concentrations of PO_4, Zn and Si are set to values of 2.17 µM, 5.4 nM (Chester and Jickells, 2012) and 92 µM respectively. Biogeochemical model simulations are initialised with these mean ocean concentrations and integrated for 5000 model years to equilibrium.

In addition to the OGCM simulations, we also conducted a suite of sensitivity tests in the 18-box ocean model CYCLOPS (Hain et al., 2014; after Keir, 1988) in which Zn cycling is linked to that of PO_4 exactly as in the OGCM. The simplicity of the box-model formulation allows us to conduct a large ensemble of 10,000 simulations with varying Zn:PO_4 uptake behaviours. As in the OGCM suite, box-model simulations are initialised with constant mean ocean concentrations of PO_4, Zn and Si as above, and integrated for 5000 model years to equilibrium. Further details are in the Supplementary Information.

3. Results and discussion

We organise the analysis and discussion of our model results as follows: in Section 3.1, we review the suite of 11 simulations presented by Vance et al. (2017), which represents the range of Zn:PO_4 uptake behaviours seen in culture data (Eqn. (1); Sunda and Huntsman, 1992) and demonstrates the importance of meridional variability in Zn:PO_4 uptake for the production of a global Zn–Si correlation. In Section 3.2, we implement 13 additional simulations to analyse the systematics of Southern Ocean Zn uptake in detail, and show that it is Zn-depletion in the Southern Ocean's Si-poor SAZ that is necessary for our model to simulate a linear Zn–Si correlation. In Section 3.3, we combine our OGCM results with a box-model ensemble to illustrate the physical mechanism by which Subantarctic depletion of Zn and Si causes these elements to be globally correlated, before discussing our results more broadly in Sections 3.4 and 3.5.

3.1. Systematics of base sensitivity simulations

In our base set of simulations (G1–G11) first presented by Vance et al. (2017), the parameters a_{Zn}, b_{Zn} and c_{Zn} in Eqn. (1) were varied to reproduce the dependency of the Zn:PO_4 uptake ratio $r_{Zn:P}$ on Zn^{2+} observed in the culturing experiments of Sunda and Huntsman (1992; Fig. 1). Note that these simulations are not meant to represent uptake by a single type of phytoplankton; rather, the culture data are used to constrain the extent to which the dependency described by Eqn. (1) may vary. Simulations G1–G11 produce what might be called a full spectrum of simulated Zn distributions, ranging from "PO_4-like" to "Si-like" (i.e., closely correlated to the simulated PO_4 or Si distribution respectively), as illustrated by the Taylor diagrams in Fig. 2a, b. In these diagrams, simulations that plot closest to the arc representing a normalised standard deviation of 1 and the radial line representing a correlation coefficient of 1 (i.e. the "bulls-eye" symbol in Fig. 2) show the greatest similarity between their three-dimensional Zn distribution and that of Si (Fig. 2a) or PO_4 (Fig. 2b). Thus whilst simulation G1 produces a Zn distribution that mimics that of PO_4, the Zn distribution of simulation G11 is highly correlated to the model's distribution of Si, with a normalised standard deviation of ~1 and a correlation coefficient of ~0.97 (Fig. 2a). Basin-average depth profiles (Fig. 3a–d) show the exceptional degree of similarity between the Zn and Si distributions in G11, which also reproduces the observed linear Zn–Si correlation in the global ocean (Fig. S3).

Table 1
Parameter values in OGCM simulations. See Supplementary Information for more details.

Simulation	Model variant	Description	Key parameter values			$\hat{E}'$	
			m_{Zn} (mol:mol/μM)			vs. Si	vs. PO_4
G1	LIN	0.25× standard slope	0.339			0.53	0.16
G2	LIN	0.5 standard slope	0.679			0.43	0.37
G3	LIN	Standard slope (∼*T. oceanica*)	1.357			0.34	0.59
G4	LIN	1.5× standard slope	2.036			0.30	0.70
G5	LIN	2× standard slope	2.714			0.27	0.77
G6	LIN	3× standard slope	4.071			0.26	0.86
			a_{Zn} (mol:mol)	b_{Zn} (μM)	c_{Zn} (mol:mol/μM)		
G7	NONLIN	Eqn. (1) fit to *E. huxleyi* A1383	2.4×10^{-3}	4.0×10^{-5}	4.7	0.30	0.71
G8	NONLIN	Eqn. (1) fit to *T. weissflogii*	1.6×10^{-3}	1.7×10^{-5}	4.0	0.32	0.66
G9	NONLIN	Eqn. (1) fit to *T. oceanica*	1.25×10^{-3}	1.0×10^{-5}	2.9	0.35	0.6
G10	NONLIN	Eqn. (1) fit to *T. pseudonana*	1.2×10^{-3}	8.0×10^{-6}	1.7	0.39	0.52
G11	NONLIN	Eqn. (1) fit to *E. huxleyi* BT6	6.0×10^{-3}	3.0×10^{-5}	0.32	0.26	0.81
G12	NONLIN	*aLO*	*1.2* $\times 10^{-3}$	1.0×10^{-5}	2.9	0.35	0.59
G13	NONLIN	*aMID*	*2.4*i $\times 10^{-3}$	1.0×10^{-5}	2.9	0.30	0.71
G14	NONLIN	*aHI*	*6.0* $\times 10^{-3}$	1.0×10^{-5}	2.9	0.24	0.90
G15	NONLIN	*bLO*	1.25×10^{-3}	*8.0* $\times 10^{-6}$	2.9	0.35	0.61
G16	NONLIN	*bMID*	1.25×10^{-3}	*3.0* $\times 10^{-5}$	2.9	0.35	0.57
G17	NONLIN	*bHI*	1.25×10^{-3}	*4.0* $\times 10^{-5}$	2.9	0.35	0.56
G18	NONLIN	*cLO*	1.25×10^{-3}	1.0×10^{-5}	*0.32*	0.45	0.36
G19	NONLIN	*cMID*	1.25×10^{-3}	1.0×10^{-5}	*1.7*	0.39	0.53
G20	NONLIN	*cHI*	1.25×10^{-3}	1.0×10^{-5}	*4.7*	0.32	0.67
G21	NONLIN	*aLO-cLO*	1.2×10^{-3}	1.0×10^{-5}	0.32	0.45	0.34
G22	NONLIN	*aHI–cLO*	6.0×10^{-3}	1.0×10^{-5}	0.32	0.25	0.85
G23	NONLIN	*aLO-cHI*	1.2×10^{-3}	1.0×10^{-5}	4.7	0.32	0.66
G24	NONLIN	*aHI–cHI*	6.0×10^{-3}	1.0×10^{-5}	4.7	0.25	0.92

$\hat{E}'$ is the normalised centred root-mean-square difference between the volume-weighted Zn field and the simulated reference field (Si or PO_4). It is defined as $\hat{E}' = E'/\sigma_r$, where σ_r is the volume-weighted standard deviation of the reference field and $E' = \{\sum \frac{V_n}{V_{tot}}[(f_n - \overline{f}) - (r_n - \overline{r})]^2\}^{1/2}$, where f represents the Zn field, r the reference field, V_n is the volume of the model cell with Zn concentration f_n, V_{tot} is total volume, and the overbar represents the volume-weighted mean (cf. Taylor, 2001).

As noted by Vance et al. (2017), these results demonstrate that given specific Zn:PO_4 uptake formulations, a linear Zn–Si relationship can be achieved despite the difference between the regeneration length-scales of Zn and Si that is built into our model. The preferential shallow remineralisation of Zn manifests in the depth profiles of Fig. 3 only as a slight enrichment relative to Si within the uppermost 1 km.

The PO_4 profile included for reference in Fig. 3a hints at the main control on the simulated Zn distribution: since Zn and PO_4 are regenerated identically in our model, the marked difference between their simulated distributions *must* come about due to differences in their relative uptake in the surface ocean. Indeed, the observed Zn–Si correlation is best reproduced by simulations in which there is significant meridional variability in the Zn:PO_4 uptake ratio $r_{Zn:P}$. This is shown for two contrasting simulations in Fig. 4. Simulation G10 only poorly reproduces the large-scale Zn–Si correlation (Figs. 2a, b and S4), and simulates Southern Ocean Zn concentrations >1 nM as far north as ∼40°S (Fig. 4a), i.e. 10° further north than in observations (Zhao et al., 2014). In contrast, in simulation G11 (Fig. 4b), which produces a Zn distribution closely correlated to that of Si (Figs. 2 and 3), surface Southern Ocean Zn concentrations decrease strongly towards the north, with a sharp gradient centred around 47°S in zonal average (Fig. S5a). This sharp gradient is the result of the uniformly high values of $r_{Zn:P}$ at high southern latitudes, which average ∼6 mmol/mol south of 47°S (Figs. 4d and S5b). Such a step-like behaviour between the mid- and high-latitude oceans is in marked contrast to the gradual poleward increase of $r_{Zn:P}$ in G10 (Fig. 4c), in which $r_{Zn:P}$ never exceeds 4 mmol/mol. As a result, in simulation G11, Zn- and macronutrient-rich deep waters that upwell to the surface Southern Ocean in the far south experience a consistently strong Zn drawdown as they are transported northwards by the simulated Ekman drift, whereas in G10, $r_{Zn:P}$ is lower and decreases steadily during the northward transport of Zn-rich surface waters. Analogous differences are visible in the subpolar North Atlantic and North Pacific, whilst in the equatorial Pacific the opposite is true: values of $r_{Zn:P}$ are elevated in simulation G10 relative to G11 (Fig. 4c, d), reflecting the unrealistically high surface Zn concentrations there (Fig. 4a).

Our base set of simulations thus shows that the observed correlation between the large-scale distributions of Zn and Si can be reproduced even in the absence of any explicit coupling between the two elements, provided that there is sufficient meridional variability in $r_{Zn:P}$. In the following, we go beyond the analysis of Vance et al. (2017) and identify the mechanisms through which this surface uptake influences the global Zn distribution, considering biological and physical controls in Sections 3.2 and 3.3 respectively.

3.2. The role of biological uptake: spatial variability of $r_{Zn:P}$

We take a systematic look at the effect of $r_{Zn:P}$ variability on the global Zn distribution using a suite of 13 sensitivity experiments in which the values of the parameters a_{Zn}, b_{Zn} and c_{Zn} in Eqn. (1) are individually varied within the bounds of the observational constraints (Sunda and Huntsman, 1992; Table 1). A first suite of 9 simulations (G12–G20) revealed that the Zn distribution is most sensitive to the parameters a_{Zn} and c_{Zn}, whilst its sensitivity to b_{Zn} is minor (Fig. S6). In the following, we thus focus on the systematics of four sensitivity simulations (G21–G24) in which permutations of the maximum and minimum values of a_{Zn} and c_{Zn} are applied, whilst b_{Zn} remains constant at a mid-range value: for clarity, we refer to these simulations as *aLO–cLO*, *aLO-cHI*, *aHI–cLO*, and *aHI–cHI* (Table 1). Fig. 2c,d demonstrates that these four simulations span the entire range of Zn–Si relationships seen in the base set of simulations. Low values of both

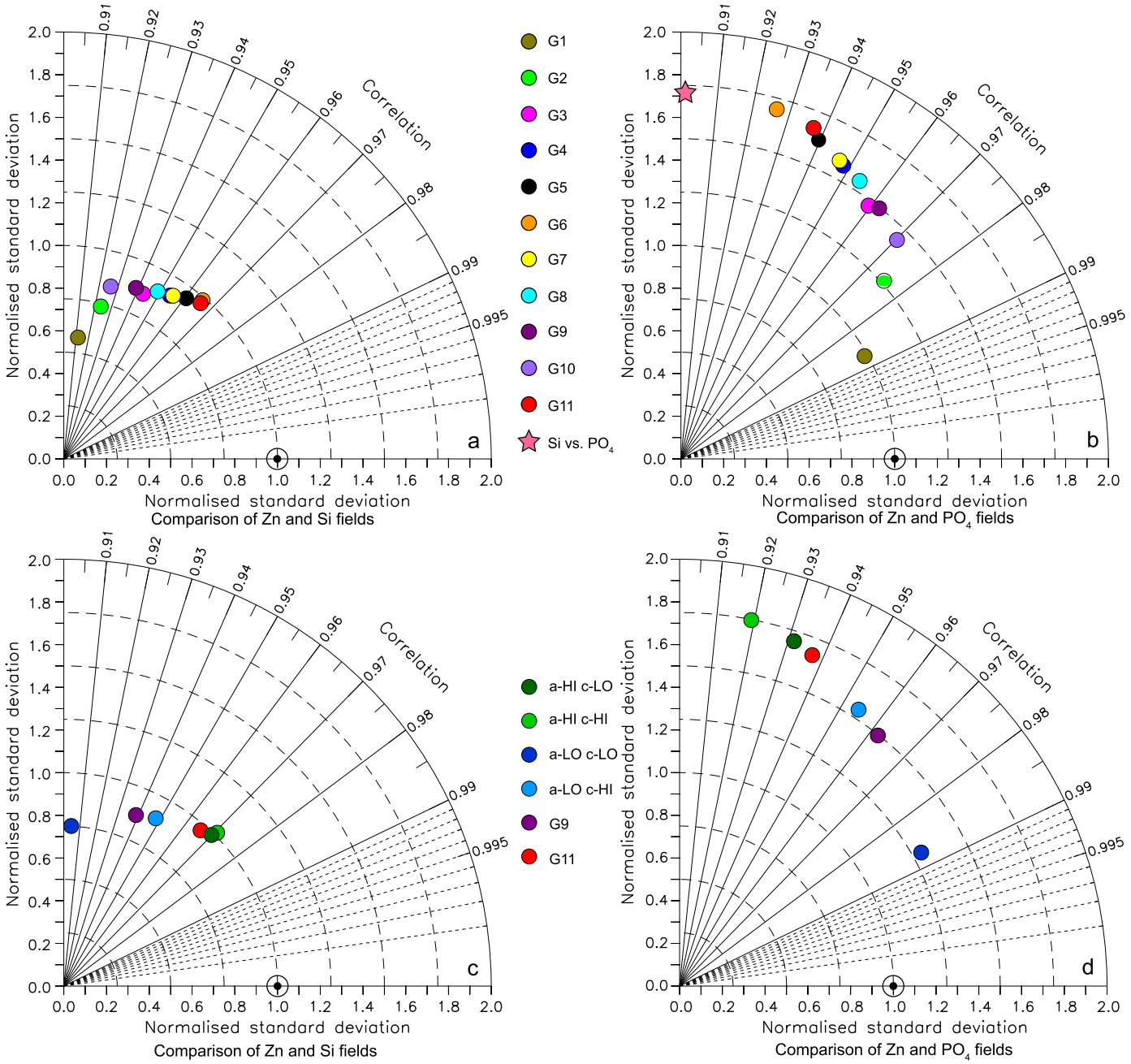

Fig. 2. Taylor diagrams illustrating the degree of similarity between the simulated Zn field and (*a, c*) the simulated Si field or (*b, d*) the simulated PO_4 field. Upper panels show results for the base set of simulations G1–G11; lower panels show results for the simulations G21–G24 (simulations G9 and G11 are included as reference). The pink star in panel *b* represents the similarity between simulated Si and PO_4 fields for reference. The bulls-eye symbol at (1, 1) represents the point at which both fields being compared are statistically identical.

a_{Zn} and c_{Zn} (*aLO–cLO*) produce poor similarity between the Zn and Si distributions (Fig. 2c). Increasing the value of c_{Zn} (*aLO-cHI*) improves the similarity of the Zn and Si fields, and increasing the value of both parameters leads to yet greater similarity (*aHI–cHI*). Interestingly, however, when a_{Zn} is high, reducing c_{Zn} to its minimum value results in barely any decrease in the similarity between global Zn and Si fields (*aHI–cLO*). Thus, a high value of a_{Zn} alone is sufficient to produce a close similarity between the Zn and Si distributions, but a high value of c_{Zn} is not. In the following, we explore the role of parameter a_{Zn} in more detail by investigating its influence on the spatial distribution of the Zn:PO_4 uptake ratio $r_{Zn:P}$.

Surface maps of $r_{Zn:P}$ (Fig. 5) reveal that when values of both a_{Zn} and c_{Zn} are low, $r_{Zn:P}$ barely shows any spatial variability (Fig. 5a). Since Zn is also regenerated identically to PO_4 in our model, it follows that the large-scale Zn distribution in *aLO–cLO* is rather similar to the PO_4 distribution (Fig. 2d). In contrast, a high value of one or both of these parameters leads to a pronounced meridional gradient in $r_{Zn:P}$ (Fig. 5b–d), with $r_{Zn:P}$ values far exceeding the mean-ocean Zn:PO_4 ratio of ∼2.5 mmol/mol in the Southern Ocean and other polar regions. However, the meridional gradients that result from high values of a_{Zn} or c_{Zn} differ considerably: a high value of c_{Zn} produces a gradual poleward increase in $r_{Zn:P}$ (Fig. 5b), whilst a high a_{Zn}-value leads to a sharply-defined step towards the poles, e.g. around 40°S in the Southern Ocean (Fig. 5c). The sensitivity of $r_{Zn:P}$ to a high a_{Zn}-value is seen most clearly in the SAZ of the Pacific Ocean (white stippling in Fig. 5c), where a high a_{Zn}-value elevates $r_{Zn:P}$ relative to simulations with

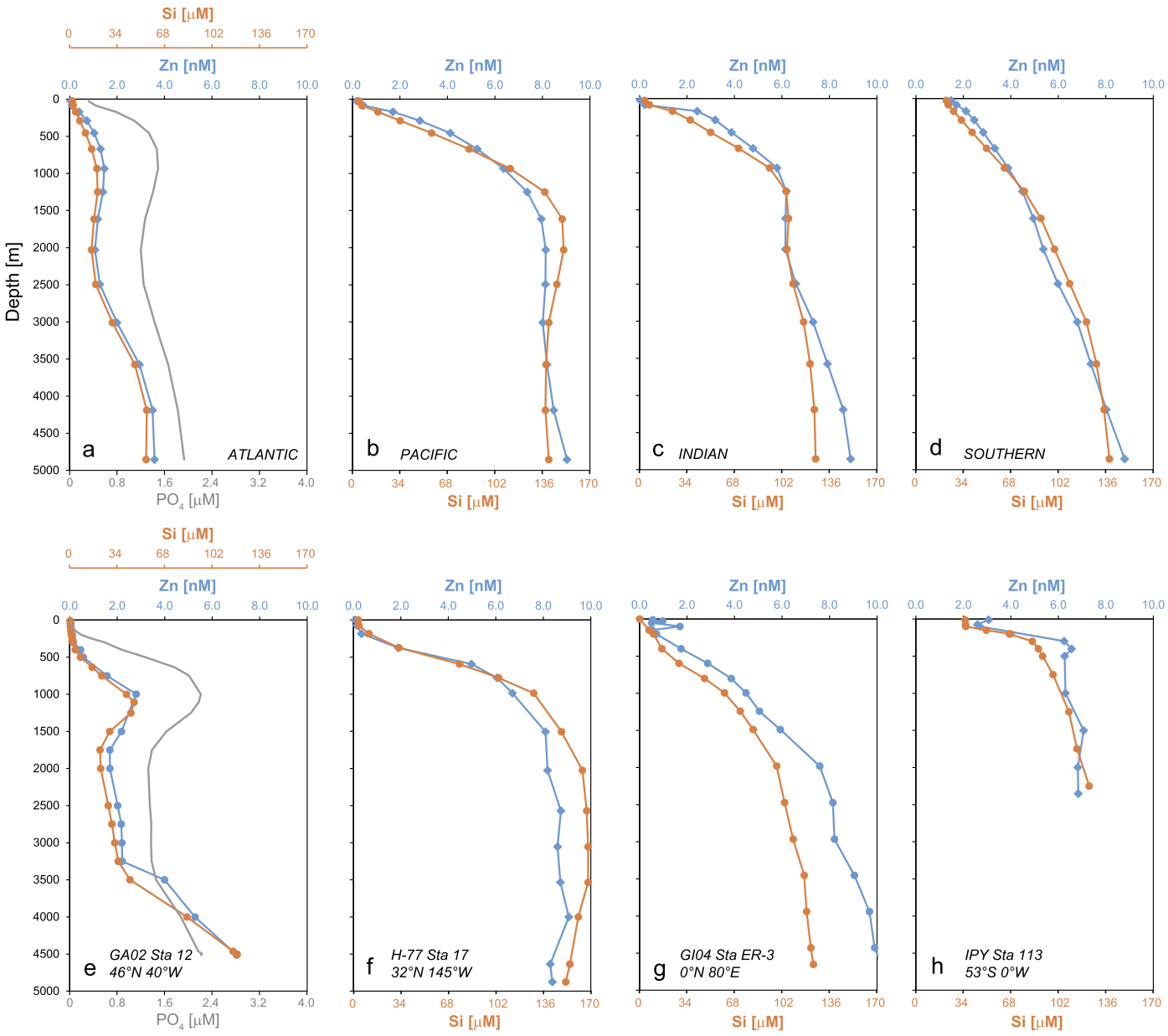

Fig. 3. Basin-average depth profiles produced by (*a–d*) simulation G11, in which the global Zn–Si relationship is well reproduced. The preferential shallow remineralisation of Zn is visible in all profiles, but only as a minor enrichment of Zn relative to Si in the upper ocean. In panel *a*, the basin-average PO_4 profile for the Atlantic basin is also shown, in order to show the degree of difference between the Zn and PO_4 fields, despite the fact that our model couples their uptake and regeneration (see Section 2 of the main text). Panels *e–h* present observational data for selected stations within each ocean basin for comparison. Data are from Bruland (1980), Zhao et al. (2014) and Mawji et al. (2015).

low values of a_{Zn} (Fig. 5a, b). The reason for the different responses of $r_{Zn:P}$ to changes in a_{Zn} and c_{Zn} becomes clear if we recall Eqn. (1) and the effects of parameter changes on the shape of the function (Fig. 1b): a_{Zn} controls the maximum value of $r_{Zn:P}$ in the non-linear, saturating Michaelis–Menten term, whilst c_{Zn} represents the non-saturating, linear increase of $r_{Zn:P}$ with Zn^{2+}. A high a_{Zn}-value thus produces a strong sensitivity of $r_{Zn:P}$ to even small amounts of Zn^{2+}. This sensitivity produces a sharp poleward shift to high and relatively constant $r_{Zn:P}$ in high-latitude regions, where upwelling of Zn-rich waters leads to elevated Zn^{2+} in the surface. The linear influence of a high c_{Zn}-value, on the other hand, produces a steady poleward gradient of $r_{Zn:P}$, such that $r_{Zn:P}$ varies *within* high-latitude regions, and especially in the Southern Ocean (Fig. 5b, d).

The consequences of the resulting differences in the Zn stoichiometry of uptake are clearly seen in the surface distribution of Zn, shown as zonal averages in Fig. 6. If we compare the Zn distributions produced by simulations *aLO–cLO* and *aHI–cLO*, it becomes clear that in the Southern Ocean, the main consequence of an elevated a_{Zn} value is a strong southward shift of the latitude at which surface Zn is nearly completely consumed. This southward shift is due to the non-linear effect of a_{Zn} discussed above, which produces high $r_{Zn:P}$ even at low Zn^{2+} concentrations, such that Zn continues to be strongly drawn down as Southern Ocean surface waters are transported northwards, even when they become significantly depleted in Zn and Zn^{2+}. As a result, Zn concentrations south of 40°S are reduced by over 1 nM in *aHI–cLO* relative to *aLO–cLO*, producing a surface Zn distribution that more closely matches the surface Si distribution than that of PO_4. Thus in simulation *aHI–cLO*, the Southern Ocean's SAZ (centred around 45°S) is strongly Zn-depleted, consistent with observations (Zhao et al., 2014).

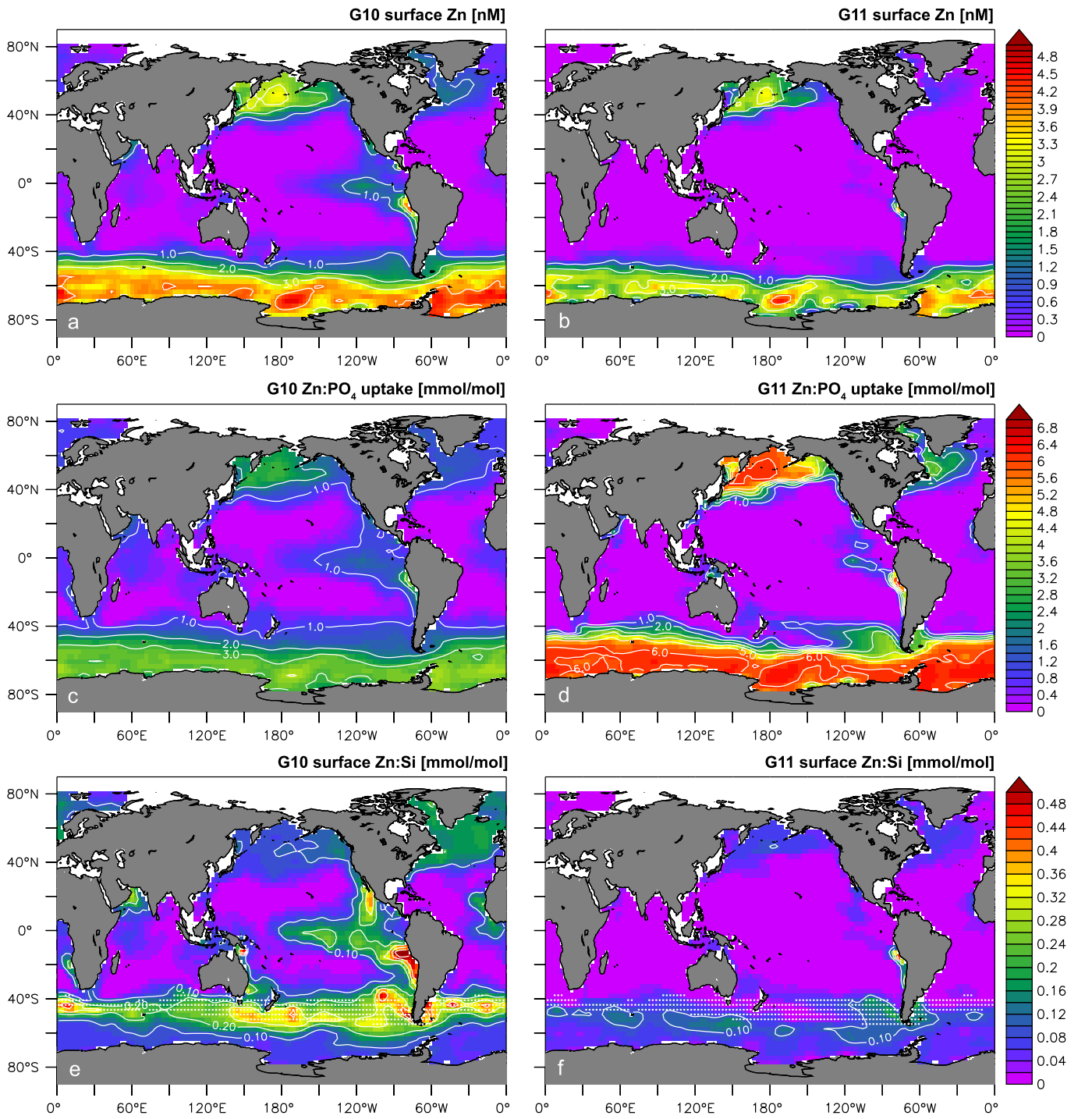

Fig. 4. Maps of (*a*, *b*) surface Zn concentration, (*c*, *d*) Zn:PO_4 uptake ratio, and (*e*, *f*) surface Zn:Si ratio in simulation G10 (left panels) and G11 (right panels). Simulation G10 is less skillful at reproducing a Si-like Zn distribution than G11 (Fig. 2), reflected e.g. by the elevation of surface Zn concentrations in the eastern equatorial Pacific Ocean (panel *a*). Panel *c* shows the relatively low Zn:PO_4 uptake ratios simulated by G10 in the high-latitude oceans, in contrast to the high ratios in simulation G11 (panel *d*). As a result, G10 shows a strong increase in the Zn:Si ratio from the Antarctic to the Subantarctic zone (panel *e*), whereas the surface Southern Ocean has a relatively homogeneous Zn:Si ratio in G11 (panel *f*). The Subantarctic Zone is indicated by white stippling in panels *e* and *f*.

Our sensitivity simulations thus demonstrate that (a) high values of the parameter a_{Zn} play the most important role in producing a close similarity between the large-scale Zn and Si distributions simulated by our OGCM, and that (b) the dominant surface–ocean effect of high a_{Zn}-values is to alter the surface Zn distribution in the Southern Ocean, particularly by reducing Zn concentrations in the SAZ. Taken together, these observations suggest a link between Subantarctic Zn depletion and the linear Zn–Si relationship in the global ocean. Below, we take advantage of the computational efficiency of the 18-box model CYCLOPS (Hain et al., 2014) to test this hypothesis.

3.3. Linking regional uptake to global distributions via the circulation

In a large ensemble of 10,000 CYCLOPS simulations, the maximum Zn:PO_4 uptake ratio $r_{Zn:P}$ in each of the model's 8 surface ocean boxes was allowed to vary, randomly and independently, between 0 and 7 mmol/mol. This ensemble reveals a systematic

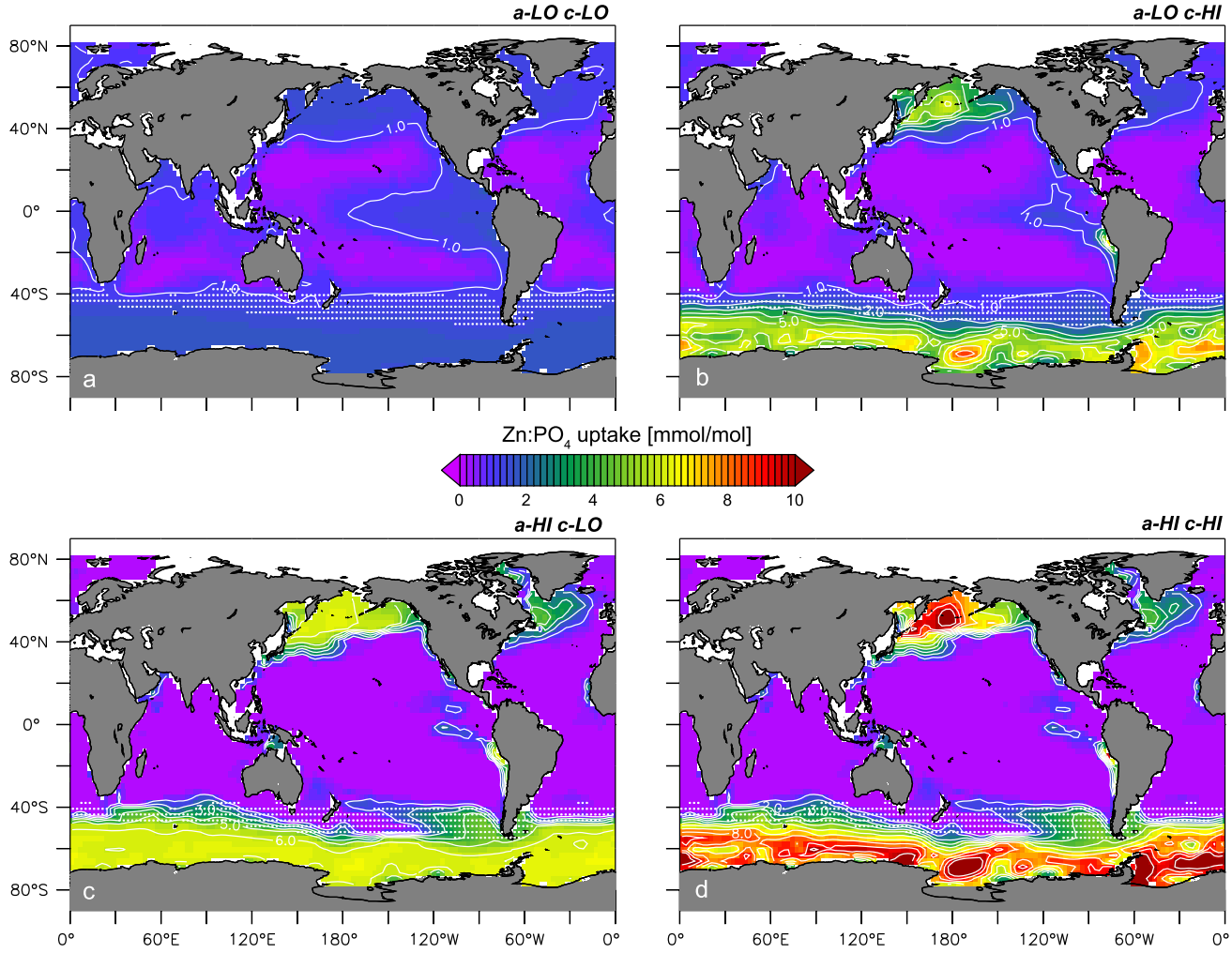

Fig. 5. Maps of Zn:PO_4 uptake ratios in simulations G21–G24, illustrating the effects of varying parameters a_{Zn} and c_{Zn} of Eqn. (1). It can be seen that whilst a high c_{Zn} -value can lead to elevated uptake at high latitudes (panels *a*, *b*), only a high a_{Zn}-value produces a step-like increase in the Subantarctic Ocean (panels *c*, *d*). The Subantarctic Zone is indicated by white stippling.

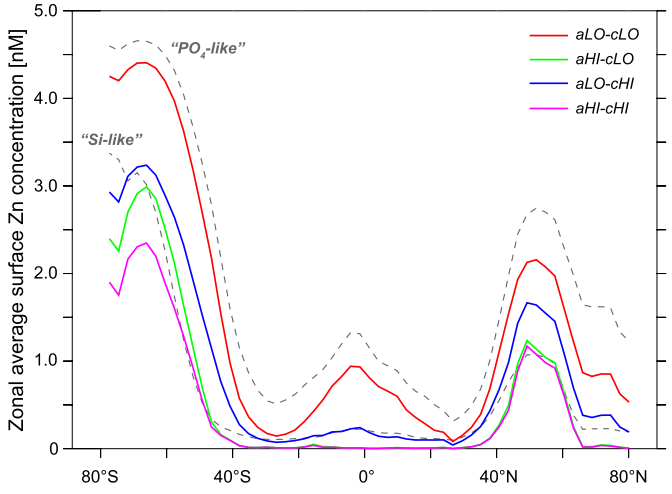

Fig. 6. Zonal average surface Zn concentrations simulated in G21–G24, in which the values of parameters a_{Zn} and c_{Zn} of Eqn. (1) are systematically varied. Dashed grey lines represent two endmember behaviours in which Zn behaves exactly like either PO_4 or Si, produced by scaling the simulated surface PO_4 (or Si) distribution by the Zn:PO_4 (or Zn:Si) ratio of the oceanic inventories. The difference between simulation *aHI–cLO* and *aLO–cLO* shows the influence of elevated values of a_{Zn} on the surface Zn distribution, resulting in a decrease of Zn concentrations in the Subantarctic Zone (∼40–50°S) to low values and a poleward migration of the meridional Zn gradients between the high- and mid-latitudes.

response of the model's SAZ to changes in Zn:PO_4 uptake stoichiometry in the Southern Ocean.

As in the real ocean, the SAZ in CYCLOPS is fed from the south by the northward transport of surface waters from the Antarctic Zone, where deep-water upwelling occurs; and it is from the SAZ that the model's upper ocean boxes are ventilated (Fig. S1). The response of the SAZ to changes in $r_{Zn:P}$ is best illustrated by its Zn:Si ratio, which reflects the degree of similarity between the behaviour of Zn and Si. The Zn:Si ratio of the SAZ reacts strongly to changes in $r_{Zn:P}$ in the Antarctic and Subantarctic surface: when Zn uptake is muted by low $r_{Zn:P}$, the Zn:Si ratio of waters upwelled to the surface Southern Ocean rises as they are transported northward into the SAZ, since Si is consumed more rapidly than Zn (Fig. 7a). When $r_{Zn:P}$ is high, however, the Zn uptake keeps pace with the strong stripping out of Si, preventing the Zn:Si ratio of surface waters from rising, and leading to a SAZ that is both Zn- and Si-depleted. As a result, at $r_{Zn:P}$ values around 5.5 mmol/mol, the congruent depletion of Zn and Si produces a Subantarctic Zn:Si ratio very similar to the mean-ocean value of ∼0.06 mmol/mol (Fig. 7a). These simulations with high Southern Ocean $r_{Zn:P}$ also exhibit the closest linear correlation between the simulated global-ocean distributions of Zn and Si, reflected by correlation coefficients close to unity in Fig. 7c. The box-model ensemble thus best reproduces the observed linear Zn–Si correlation when SAZ Zn:Si ratios are close to the global-ocean mean (Fig. 7e).

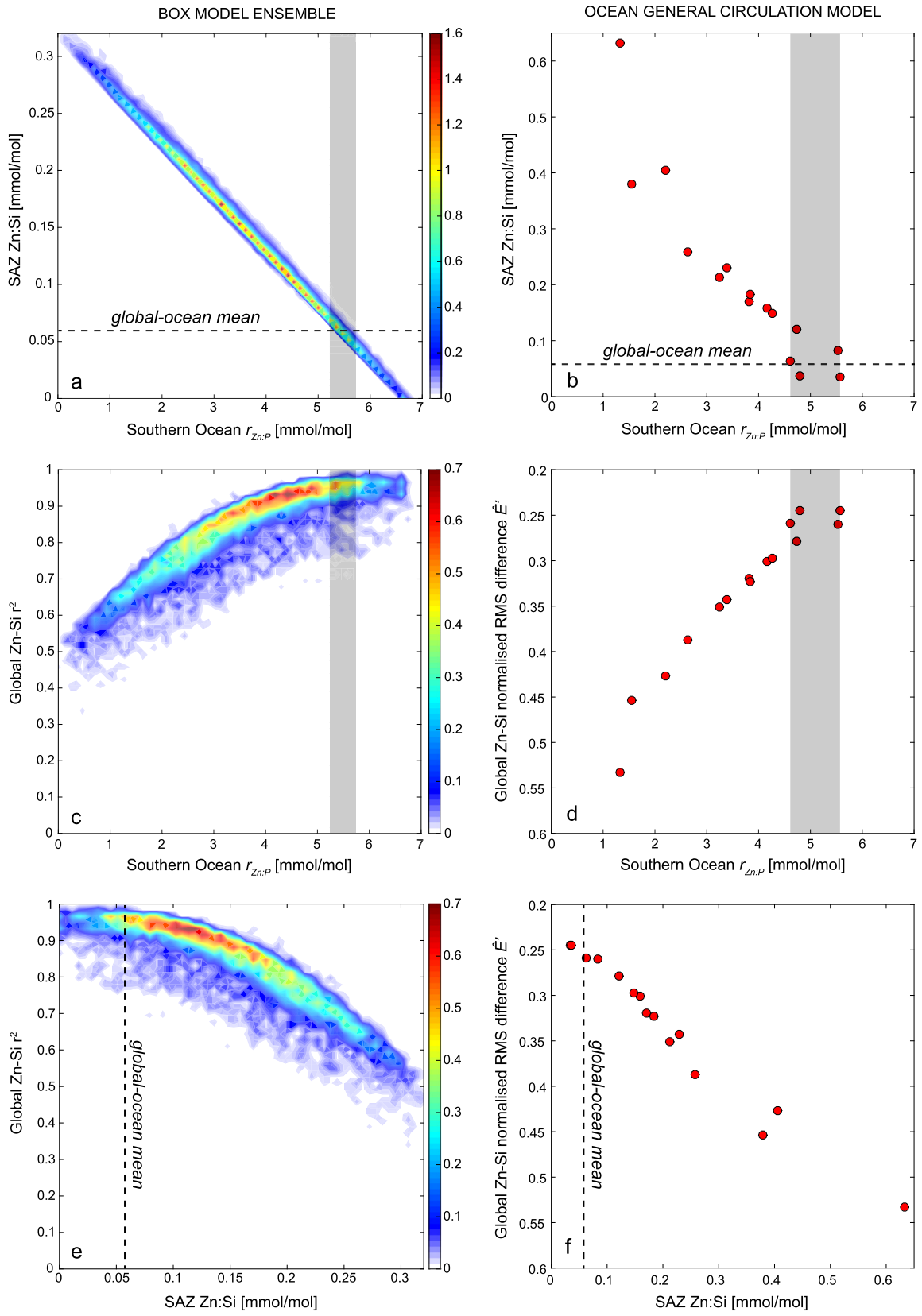

Fig. 7. Sensitivity simulation systematics in (*a, c, e*) the box-model ensemble and (*b, d, f*) OGCM simulations (G1–G11, G21–G24). Box-model ensemble results are shown as density maps of the percentage of ensemble members with the given *x*, *y* characteristics. Panels *a* and *b* show that higher Southern Ocean Zn:PO_4 uptake (i.e. the model's Antarctic and Subantarctic boxes) results in a steady decrease in Zn:Si in Subantarctic waters, with values approaching the global-ocean mean (dashed line) when Southern Ocean Zn:PO_4 uptake is ~5.5 mmol/mol. Vertical grey bars mark the range of Southern Ocean $r_{Zn:P}$ that produce a SAZ Zn:Si ratio close to the global-ocean mean. Panels *c* and *d* show metrics for the similarity between the resulting Zn and Si tracer fields (correlation coefficient r^2 or normalised centred root-mean-square difference $\hat{E}'$, defined in Table 1; note reversed *y*-axis in *d* and *e*). Panels *e* and *f* show that as the surface Subantarctic Zn:Si approaches the global mean, the similarity between the simulated Zn and Si tracer fields increases towards its highest values.

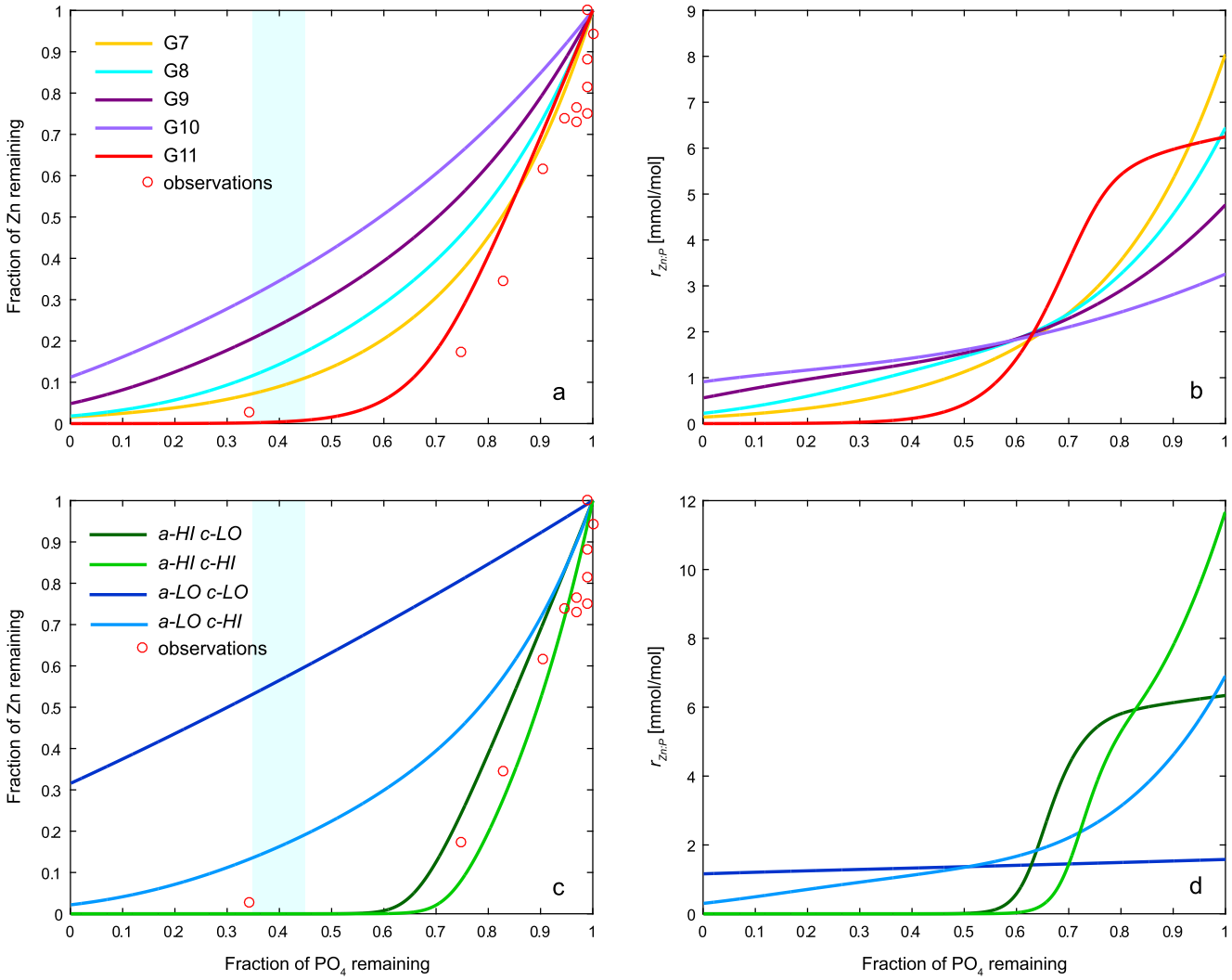

Fig. 8. Systematics of relative Zn and PO_4 drawdown produced by the parameter choices for Eqn. (1) in the OGCM sensitivity simulations. Panels *a* and *c* show the residual Zn as a function of residual PO_4, whilst panels *b* and *d* show the $r_{Zn:P}$ uptake ratios that lead to this relationship. Red circles represent observations in the surface Southern Ocean along the prime meridian by Zhao et al. (2014), normalised to the maximum concentrations of Zn and PO_4 observed along the section (3.7 nM and 1.85 μM respectively) at the Antarctic Divergence. These values were also used as the initial conditions for the calculation of Zn drawdown using Eqn. (1). The vertical blue bar at a residual PO_4 fraction of 40%, the value observed in the SAZ, highlights the range in Zn drawdown produced by the different parameter choices. Note the close correspondence between the degree of drawdown of Zn and model skill at reproducing the global Zn–Si relationship (cf. Fig. 2).

The intuition gained from the box-model systematics can be directly applied to our OGCM simulations. The right-hand panels of Fig. 7 show results for simulations G1-11 and G21–24 analogous to those presented for the box model. From Fig. 7b, it is clear that here too, an increase of Southern Ocean $r_{Zn:P}$ leads to a strong decrease in the Zn:Si ratio of the SAZ. Simulations with low Southern Ocean $r_{Zn:P}$ produce a Subantarctic surface highly enriched in Zn relative to Si, and fare worst in reproducing the global Zn–Si correlation (Fig. 7d). Conversely, simulations in which high Southern Ocean $r_{Zn:P}$ leads to a Subantarctic Zn:Si ratio close to the mean-ocean value produce the best match between the global Zn and Si fields (Fig. 7f).

The systematics of the box-model ensemble and OGCM thus strongly support the hypothesis that Southern Ocean Zn uptake exerts its control on the global Zn–Si relationship via its influence on Subantarctic Zn status: Figs. 7e–f make it clear that high degrees of correlation between the global Zn and Si fields correspond to SAZ Zn:Si ratios close to the mean-ocean value. Given that a linear Zn–Si relationship implies a constant Zn:Si ratio in the interior ocean, this correspondence suggests that the SAZ is important for the global correlation since it determines the preformed Zn:Si ratio of SAMW and AAIW, water masses of near-global importance that are subducted from the SAZ and ventilate the basal-thermocline and intermediate ocean (Hanawa and Talley, 2001; Sallée et al., 2010), as previously suggested by Ellwood (2008) and Wyatt et al. (2014). Indeed, in our OGCM simulations, the Zn:Si ratio along an isopycnal corresponding to SAMW in the Atlantic Ocean ($\sigma_\theta = 26.8$ kg/m^3), which outcrops in the SAZ near 45°S in the OGCM, responds sensitively to the $r_{Zn:P}$ value of Southern Ocean uptake: as with the Subantarctic surface from which it is ventilated, the Zn:Si ratio on this isopycnal falls to values close the mean-ocean ratio with elevated Southern Ocean Zn uptake. This ratio also correlates exceptionally strongly with the root-mean-square difference between the global Zn and Si distributions ($r^2 = 0.99$; Fig. S7): the marine Zn and Si distributions are most similar when the Zn:Si ratio on this isopycnal is closest to the mean-ocean ratio. Taken together, these interrelationships show that the biogeochemical properties of the upper-ocean water masses ventilated from the SAZ are the decisive element in creating a close correlation between the global marine Zn and Si distributions, by transposing the low-Zn, low-Si signature of the surface SAZ into the interior.

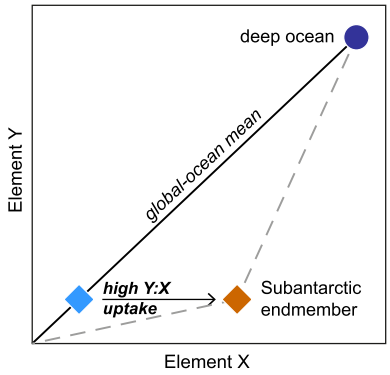

Fig. 9. Cartoon illustrating a potential mechanism for Subantarctic control of global marine elemental correlations. If element *Y* is more strongly depleted than element *X* in the Subantarctic Zone relative to their mean-ocean ratio, the low-concentration endmember subducted into the interior from the Subantarctic will lie below the line connecting the deep ocean and the origin (orange diamond). Circulation and mixing of these upper-ocean water masses will produce the concave-upward relationship seen e.g. between Zn and PO_4 in the global ocean (dashed lines). The blue diamond represents the case in which both elements are present in approximately their global-ocean mean ratio in upper-ocean waters subducted from the Subantarctic, leading to a close-to-linear relationship at the global scale, as for Zn and Si.

3.4. General systematics of the Subantarctic control

The discussion in Sections 3.2 and 3.3 above has clearly shown the importance of Subantarctic surface properties for the global Zn distribution, and the physical mechanism by which this control comes about. We now attempt to gain a more generalised understanding of the Subantarctic control on the large-scale distribution of Zn and biologically-cycled elements in general.

We first consider the biological drawdown of Zn and PO_4 in the surface Southern Ocean. Results discussed in Section 3.2 demonstrated that it is Zn-depletion in the Subantarctic that is key to reproducing the observed Zn–Si correlation. We apply a simple generalised framework to assess the relative Southern Ocean drawdown of Zn and PO_4 simulated by our sensitivity suite, building upon the fact that PO_4 concentrations in the Subantarctic Zone are only ∼40% of those in Antarctic waters south of the Polar Front (Garcia et al., 2013). If we make the simplifying assumption that all nutrient supply to the SAZ comes through Ekman transport from the south, then in order to produce a Subantarctic surface depleted in Zn, Southern Ocean Zn drawdown must be sufficiently strong to produce Zn-depletion when PO_4 has been drawn down to only 40% of its initial Antarctic value. We thus calculate the expected relationship between the drawdown of Zn and PO_4 that results from the parameter choices for the equation governing $r_{Zn:P}$ (Eqn. (1)) in our OGCM sensitivity suite. In Fig. 8, it can be seen that when PO_4 has been drawn down to 40% of its initial Antarctic concentration, the simulated fraction of residual Zn varies between ∼0% and ∼60%. Those simulations that draw down Zn most strongly (G11, *aHI–cLO*, *aHI–cHI*), depleting Zn when residual PO_4 is at 40% or more, best reproduce the observed covariation between Zn and PO_4 in the surface Southern Ocean (Fig. 8; Zhao et al., 2014). Tellingly, it is these same simulations that best reproduce the global linear relationship between Zn and Si (Fig. 2). This general framework thus shows that a key variable in determining Subantarctic Zn status, and thus the large-scale Zn distribution, is the *integrated* Zn:PO_4 uptake ratio experienced by surface Southern Ocean water masses as they are transported northwards to the Subantarctic Zone.

Secondly, whilst in the case of Zn it is *depletion* in the Subantarctic surface that is a key prerequisite to correctly simulating the Zn–Si and Zn–PO_4 relationships, the systematics of our box-model ensemble offer the tantalising suggestion that this might be only one specific case of a coupled biological–physical Subantarctic mechanism that explains elemental correlations in the sea more generally. As discussed in Section 3.3, box-model simulations in which high $r_{Zn:P}$ values lead to strong Zn drawdown have a Subantarctic Zn:Si ratio very similar to the global-ocean mean (Fig. 7a), and hence strongly correlated Zn and Si distributions. Analysis of the Zn:PO_4 systematics of the ensemble shows that the simulated Zn distribution becomes, instead, almost perfectly linearly correlated with PO_4 when the Zn:PO_4 ratio in the SAZ equals the mean-ocean Zn:PO_4 ratio of ∼2.5 mmol/mol (Fig. S8). The analogous existence of such a link between Subantarctic elemental stoichiometry and global distributions for both Zn–Si *and* Zn–PO_4 suggests a more general mechanism of Subantarctic control. The ventilation of the upper-ocean water masses SAMW and AAIW from the Subantarctic introduces its surface stoichiometric signal into the ocean interior, setting the preformed stoichiometry of the upper ocean (Fig. 9). If this upper-ocean "endmember", with low elemental concentrations, bears the same stoichiometric ratio between two elements as the nutrient-rich deep ocean that influences the global mean, the global relationship between these two elements will be near-linear (Fig. 9), as in the case of Zn and Si in the modern ocean. If, in contrast, Southern Ocean uptake leads to a strong relative depletion in one of these elements in the Subantarctic surface, the low-concentration endmember subducted from the Subantarctic will bear a lower elemental ratio than the nutrient-rich deep ocean, a ratio that is imparted not only to the thermocline but also to the formation regions of nutrient-poor North Atlantic Deep Water, via the cross-equatorial transport of SAMW/AAIW (de Souza et al., 2015). As a result, the global relationship between the two elements will be convex-upwards (Fig. 9), with a steep relationship representing mixing between Subantarctic-sourced upper-ocean waters and the nutrient-rich deep ocean – as in the case of Zn and PO_4 in the ocean (Fig. S3) or, indeed, Si and PO_4.

3.5. Synthesis and broader implications

The discussion above has highlighted the extent to which Southern Ocean Zn uptake plays a role in determining the global Zn distribution. Specifically, the OGCM results presented in Section 3.2 show that the northward extension of elevated Zn uptake into the SAZ, even as Zn and Zn^{2+} concentrations drop, is key to reproducing the observed Zn–Si correlation (Fig. 4). It must be noted that our biogeochemical model achieves this uptake via a relationship between Zn:PO_4 uptake ratios and Zn^{2+} (Eqn. (1)) that is certainly an oversimplification of the complexity of marine Zn biogeochemistry (e.g. Varela et al., 2011). The surface distribution of Zn^{2+} is sensitive to the concentration and distribution of the chelating ligand that binds most dissolved Zn. Ligand-sensitivity simulations show that the specifics of our results are dependent on the absolute value of this parameter (Fig. S10). However, our analysis has focused on the systematics of our sensitivity suite, which is unaffected by such specifics (Fig. S10). This approach has allowed us to identify macro-scale biogeochemical processes that are associated with the simulation of a more realistic marine Zn distribution, and it is on this process understanding that we focus here.

Whilst at the global scale the production of a Zn-depleted Subantarctic surface seems to be a sufficient condition for reproducing the Zn distribution, at the regional scale additional nuances appear. Simulations *aHI–cLO* and *aHI–cHI*, for instance, demonstrate similar global skill (Fig. 2c, d), and both produce a Zn-depleted Subantarctic surface, although Zn drawdown in *aHI–cHI* is considerably stronger than in *aHI–cLO* (Fig. 8c), as a result of the extremely high $r_{Zn:P}$ that *aHI–cHI* simulates at high Zn^{2+} concentrations (Fig. 8d). This elevated Zn uptake has consequences for the latitudinal distribution of Zn in the surface Southern Ocean simulated by *aHI–cHI*, limiting the degree to which Zn concentrations can rise in regions

of Southern Ocean upwelling centred around 60°S (Fig. 6). Thus unlike *aHI–cLO*, which reproduces the observed surface Southern Ocean covariation between Zn and Si along the prime meridian (Zhao et al., 2014) with good fidelity, *aHI–cHI* consistently underestimates Zn concentrations in the far south (Fig. S9). This difference in regional skill suggests that the step-like increase in $r_{Zn:P}$ simulated by *aHI–cLO*, with low values in the temperate latitudes and a rapid rise to a plateau of high $r_{Zn:P}$ values in the subpolar and polar oceans, better captures the variation of $r_{Zn:P}$ required to explain the Zn distribution at multiple scales, ranging from the regional to the global. Our simple biogeochemical model produces this step via what is essentially a physiological mechanism (Eqn. (1)), but the sharp separation of oceanic provinces that results suggests the possibility that such a variation might, in the real ocean, be driven instead by differences in biogeography, nutrient status or environmental conditions.

Differing Zn quotas in high- and low-latitude phytoplankton could, for instance, be the result of adaptive changes to ambient Zn concentrations within phytoplankton groups, analogous to differences in Si quota observed between high-latitude and equatorial diatoms (e.g. Baines et al., 2010); such an adaptation is indeed suggested by the lower Zn requirements observed in open-ocean phytoplankton species relative to coastal ones (Sunda and Huntsman, 1992). Alternatively, as has been previously suggested by Ellwood (2008) and Croot et al. (2011), elevated Zn quotas in high-latitude high-nutrient low-chlorophyll regions such as the Southern Ocean and subpolar North Pacific may be a response to the chronic iron limitation of phytoplankton in these regions (Chisholm and Morel, 1991), since iron limitation has been shown to elevate Zn quotas in iron-limited natural phytoplankton communities (Sunda and Huntsman, 2000; Cullen et al., 2003). Our biogeochemical model, with its prescribed dependency of $r_{Zn:P}$ on Zn^{2+}, is by construction agnostic as to the ecological and/or biochemical causes of the variation in $r_{Zn:P}$. What is clear is that model variants that produce a realistic Zn distribution also reproduce the marked difference in Zn quotas observed between Southern Ocean diatoms and low-latitude genera (Twining and Baines, 2013). In our opinion, this result strongly suggests that it is Southern Ocean diatoms that are dominantly responsible for the large-scale Zn–Si correlation in the global ocean (see also Ellwood, 2008), and that – via their extraordinary affinity for Zn and abundant seasonal blooms – they dominantly control the fluxes driving the global-scale Zn cycle. Certainly, in our most skillful model variants, Zn export fluxes south of 40°S represent 44% or more of global Zn export (Table S2), making the Southern Ocean almost as important for Zn as for Si (54%), and more than twice as important as for the export of P (19%). In this context, it is worth re-iterating that the observed levels of Zn directly incorporated into the opaline frustules of diatoms are too low to explain the marine Zn–Si correlation, as shown by simulations of coupled Zn–Si cycling discussed in the Supplementary Information.

The far-reaching consequences of elevated Southern Ocean Zn uptake are highlighted by fact that the physical model we employ simulates significant low-latitude upwelling (Resplandy et al., 2016). This simulated upwelling is patently insufficient to overcome the Zn depletion of the upper ocean that results when Zn is stripped out of the model's SAZ. With most Zn efficiently trapped in the deep ocean by the elevated Zn export fluxes of the Southern Ocean, wind-driven upwelling in coastal and equatorial regions can only tap into a relatively small Zn upper-ocean pool, most of which is likely efficiently recycled within the upper ocean due to the shallow remineralisation of organic-associated Zn (Twining et al., 2014). It would thus seem that the low-latitude cycling of Zn is dominated by a shallow recycling loop that remains rather disconnected from the large-scale, Southern-Ocean-dominated cycle determining the global Zn distribution. This raises the interesting possibility that the observed differences between the Zn quotas of eukaryotic and prokaryotic phytoplankton (e.g. Sunda and Huntsman, 1992, 1995; Saito et al., 2002; Twining et al., 2011) may also be the consequence of adaptation to ambient Zn concentrations, rather than representing a fundamental physiological difference: by sequestering Zn in the deep Southern Ocean, high-latitude eukaryotic diatom communities might effectively "starve" low-latitude phytoplankton communities, including prokaryotic cyanobacteria that thrive in the subtropics, of zinc. Whilst speculative, it appears at least possible that the lower Zn quotas observed for low-latitude cyanobacteria (e.g. Twining et al., 2011) might represent an adaptive response to this diatom-driven Zn starvation, rather than reflecting a fundamental difference in physiological demand between prokaryotes and eukaryotes (cf. Saito et al., 2003).

At the broadest scale, the correlative mechanism identified by this study has applicability beyond the marine Zn distribution. As discussed in detail in Section 3.4, the degree to which Southern Ocean uptake draws down the Subantarctic concentration of an element relative to that of PO_4 determines the upper-ocean endmember that defines the interior-ocean correlation between that element and PO_4 (Fig. 9). This mechanism should apply equally to other elements whose oceanic residence time is sufficiently long for large-scale circulation to play a significant role in determining their distribution. In this context, the much-discussed "kink" in the marine relationship between cadmium (Cd) and PO_4 would appear to result from Southern Ocean uptake that is elevated in Cd relative to PO_4, albeit to a smaller extent than is the case for Zn (cf. Baars et al., 2014). Further observations of *in situ* utilisation and phytoplankton stoichiometry, as well as modelling studies of their effects on the large-scale distribution, would allow a robust test of this hypothesis.

4. Conclusions

Vance et al. (2017) recently showed that elevated Southern Ocean uptake of Zn can produce the observed correlation between the global distributions of dissolved Zn and Si in seawater without any mechanistic links between their marine cycles. In this study, our interest has been to understand the main biological and physical mechanisms through which surface uptake in the remote Southern Ocean exercises such global influence. Our model sensitivity suites have shown that the stoichiometry of Southern Ocean Zn uptake relative to that of PO_4 controls the degree of similarity between Zn and Si distributions via its influence on the elemental stoichiometry of the Subantarctic Zone of the Southern Ocean, where water masses that fill the upper ocean are formed. Because both Si and Zn are drawn down nearly to completion before being subducted into the upper-ocean interior by SAMW/AAIW, the global ocean Zn–Si relationship comes to resemble a simple mixing line between the Zn- and Si-depleted SAMW/AAIW endmember and the high-Zn and high-Si deep ocean, with the mean ocean Zn:Si ratio determining the slope of the relationship. Furthermore, since the upper ocean holds very little of the global ocean Zn and Si inventories, the global-scale correlation set in the frontal system of the Southern Ocean cannot be undone by biological cycling in the low-latitude surface, or by differences in the remineralisation depths of Zn-bearing organic matter and opal.

Acknowledgements

We thank M. Ellwood and two anonymous reviewers for constructive reviews that helped improve a previous version of this manuscript, and M. Frank for thoughtful editorial handling. GFdS is supported by a Marie Skłodowska-Curie Research Fellowship under EU Horizon 2020 (SOSiC; 708407). MPH is supported by a NERC

Independent Research Fellowship (NE/K00901X/1). SHL acknowledges support from the Leverhulme Trust (ECF-2014-615) and the National Environment Research Council (NERC): NE/P018181/1.

Appendix A. Supplementary material

Supplementary material related to this article can be found online at https://doi.org/10.1016/j.epsl.2018.03.050.

References

Baars, O., Croot, P.L., 2011. The speciation of dissolved zinc in the Atlantic sector of the Southern Ocean. Deep Sea Res. II 58, 2720–2732.

Baars, O., Abouchami, W., Galer, S.J.G., Boye, M., Croot, P.L., 2014. Dissolved cadmium in the Southern Ocean: distribution, speciation, and relation to phosphate. Limnol. Oceanogr. 59, 385–399.

Baines, S.B., Twining, B.S., Brzezinski, M.A., Nelson, D.M., Fisher, N.S., 2010. Causes and biogeochemical implications of regional differences in silicification of marine diatoms. Glob. Biogeochem. Cycles 24, GB4031. https://doi.org/10.1029/2010gb003856.

Berelson, W.M., 2001. The flux of particulate organic carbon into the ocean interior: a comparison of four US JGOFS regional studies. Oceanography 14, 59–67.

Broecker, W.S., Peng, T.H., 1982. Tracers in the Sea. Eldigio Press/Lamont–Doherty Geological Observatory, Palisades, NY.

Bruland, K.W., 1980. Oceanographic distributions of cadmium, zinc, nickel, and copper in the North Pacific. Earth Planet. Sci. Lett. 47, 176–198.

Bruland, K.W., 1989. Complexation of zinc by natural organic ligands in the central North Pacific. Limnol. Oceanogr. 34, 269–285.

Chester, R., Jickells, T., 2012. Marine Geochemistry, 3rd ed. Wiley–Blackwell, Chichester.

Chisholm, S.W., Morel, F.M.M. (Eds.), 1991. Special Issue: What Controls Phytoplankton Production in Nutrient-Rich Areas of the Open Sea? Limnol. Oceanogr. 36, 1507–1970.

Croot, P.L., Baars, O., Streu, P., 2011. The distribution of dissolved zinc in the Atlantic sector of the Southern Ocean. Deep-Sea Res. II 58, 2707–2719.

Cullen, J.T., Chase, Z., Coale, K.H., Fitzwater, S.E., Sherrell, R.M., 2003. Effect of iron limitation on the cadmium to phosphorus ratio of natural phytoplankton assemblages from the Southern Ocean. Limnol. Oceanogr. 48, 1079–1087.

de Souza, G.F., Slater, R.D., Dunne, J.P., Sarmiento, J.L., 2014. Deconvolving the controls on the deep ocean's silicon stable isotope distribution. Earth Planet. Sci. Lett. 398, 66–76.

de Souza, G.F., Slater, R.D., Hain, M.P., Brzezinski, M.A., Sarmiento, J.L., 2015. Distal and proximal controls on the silicon stable isotope signature of North Atlantic Deep Water. Earth Planet. Sci. Lett. 432, 342–353.

Donat, J.R., Bruland, K.W., 1990. A comparison of two voltammetric techniques for determining zinc speciation in Northeast Pacific Ocean waters. Mar. Chem. 28, 301–323.

Ellwood, M.J., 2004. Zinc and cadmium speciation in Subantarctic waters east of New Zealand. Mar. Chem. 87, 37–58.

Ellwood, M.J., 2008. Wintertime trace metal (Zn, Cu, Ni, Cd, Pb and Co) and nutrient distributions in the Subantarctic Zone between 40–52°S; 155–160°E. Mar. Chem. 112, 107–117.

Ellwood, M.J., Hunter, K.A., 2000. The incorporation of zinc and iron into the frustule of the marine diatom *Thalassiosira pseudonana*. Limnol. Oceanogr. 45, 1517–1524.

Ellwood, M.J., van den Berg, C.M.G., 2000. Zinc speciation in the Northeastern Atlantic Ocean. Mar. Chem. 68, 295–306.

Garcia, H.E., Locarnini, R.A., Boyer, T.P., Antonov, J.I., Baranova, O.K., Zweng, M.M., et al., 2013. World Ocean Atlas 2013, Volume 4: Dissolved Inorganic Nutrients (Phosphate, Nitrate, Silicate). In: Levitus, S. (Ed.), NOAA Atlas NESDIS, Silver Spring, MD, p. 25.

Hain, M.P., Sigman, D.M., Haug, G.H., 2014. Distinct roles of the Southern Ocean and North Atlantic in the deglacial atmospheric radiocarbon decline. Earth Planet. Sci. Lett. 394, 198–208.

Hanawa, K., Talley, L.D., 2001. Mode waters. In: Siedler, G., Church, J.A., Gould, J. (Eds.), Ocean Circulation and Climate – Observing and Modelling the Global Ocean. Academic Press, San Diego, pp. 373–386.

Keir, R.S., 1988. On the Late Pleistocene ocean geochemistry and circulation. Paleoceanography 3, 413–455.

Khatiwala, S., Visbeck, M., Cane, M.A., 2005. Accelerated simulation of passive tracers in ocean circulation models. Ocean Model. 9, 51–69.

Lohan, M.C., Crawford, D.W., Purdie, D.A., Statham, P.J., 2005. Iron and zinc enrichments in the northeastern subarctic Pacific: ligand production and zinc availability in response to phytoplankton growth. Limnol. Oceanogr. 50, 1427–1437.

Marshall, J., Adcroft, A., Hill, C., Perelman, L., Heisey, C., 1997. A finite-volume, incompressible Navier–Stokes model for studies of the ocean on parallel computers. J. Geophys. Res., Oceans 102, 5733–5752.

Martin, J.H., Knauer, G.A., Karl, D.M., Broenkow, W.W., 1987. VERTEX: carbon cycling in the northeast Pacific. Deep Sea Res. 34, 267–285.

Mawji, E., Schlitzer, R., Dodas, E.M., Abadie, C., Abouchami, W., Anderson, R.F., et al., 2015. The GEOTRACES intermediate data product 2014. Mar. Chem. 177, 1–8.

Morel, F.M.M., Milligan, A.J., Saito, M.A., 2014. Marine bioinorganic chemistry: the role of trace metals in the oceanic cycles of major nutrients. In: Holland, H.D., Turekian, K.K. (Eds.), Treatise on Geochemistry, Second Edition. Elsevier, Oxford, pp. 123–150.

Najjar, R.G., Jin, X., Louanchi, F., Aumont, O., Caldeira, K., Doney, S.C., et al., 2007. Impact of circulation on export production, dissolved organic matter, and dissolved oxygen in the ocean: results from phase II of the Ocean Carbon-cycle Model Intercomparison Project (OCMIP-2). Glob. Biogeochem. Cycles 21. https://doi.org/10.1029/2006gb002857.

Price, J., Badger, M.R., 1989. Isolation and characterization of high CO_2-requiring mutants of the cyanobacterium *Synechococcus* PCC7942-2 phenotypes that accumulate inorganic carbon but are apparently unable to generate CO_2 within the carboxysome. Plant Physiol. 91, 514–525.

Resplandy, L., Keeling, R.F., Stephens, B.B., Bent, J.D., Jacobson, A., Rödenbeck, C., Khatiwala, S., 2016. Constraints on oceanic meridional heat transport from combined measurements of oxygen and carbon. Clim. Dyn. 47, 3335–3357.

Rueter, J.G., Morel, F.M.M., 1981. The interaction between zinc deficiency and copper toxicity as it affects the silicic acid uptake mechanisms in *Thalassiosira pseudonana*. Limnol. Oceanogr. 26, 67–73.

Saito, M.A., Moffett, J.W., Chisholm, S.W., Waterbury, J.B., 2002. Cobalt limitation and uptake in *Prochlorococcus*. Limnol. Oceanogr. 47, 1629–1636.

Saito, M.A., Sigman, D.M., Morel, F.M.M., 2003. The bioinorganic chemistry of the ancient ocean: the co-evolution of cyanobacterial metal requirements and biogeochemical cycles at the Archean–Proterozoic boundary. Inorg. Chim. Acta 356, 308–318.

Sallée, J.-B., Speer, K., Rintoul, S., Wijffels, S., 2010. Southern Ocean thermocline ventilation. J. Phys. Oceanogr. 40, 509–529.

Sarmiento, J.L., Simeon, J., Gnanadesikan, A., Gruber, N., Key, R.M., Schlitzer, R., 2007. Deep ocean biogeochemistry of silicic acid and nitrate. Glob. Biogeochem. Cycles 21. https://doi.org/10.1029/2006GB002720.

Sherbakova, T.A., Masyukova, Y.A., Safonova, T.A., Petrova, D.P., Vereshagin, A.L., Minaeva, T.V., et al., 2005. Conserved motif CMLD in silicic acid transport proteins of diatoms. Mol. Biol. 39, 269–280.

Sunda, W.G., Huntsman, S.A., 1992. Feedback interactions between zinc and phytoplankton in seawater. Limnol. Oceanogr. 37, 25–40.

Sunda, W.G., Huntsman, S.A., 1995. Cobalt and zinc interreplacement in marine phytoplankton: biological and geochemical implications. Limnol. Oceanogr. 40, 1404–1417.

Sunda, W.G., Huntsman, S.A., 2000. Effect of Zn, Mn, and Fe on Cd accumulation in phytoplankton: implications for oceanic Cd cycling. Limnol. Oceanogr. 45, 1501–1516.

Taylor, K.E., 2001. Summarizing multiple aspects of model performance in a single diagram. J. Geophys. Res., Atmos. 106, 7183–7192.

Twining, B.S., Baines, S.B., Fisher, N.S., 2004. Element stoichiometries of individual plankton cells collected during the Southern Ocean Iron Experiment (SOFeX). Limnol. Oceanogr. 49, 2115–2128.

Twining, B.S., Baines, S.B., Bozard, J.B., Vogt, S., Walker, E.A., Nelson, D.M., 2011. Metal quotas of plankton in the equatorial Pacific Ocean. Deep-Sea Res. II 58, 325–341.

Twining, B.S., Baines, S.B., 2013. The trace metal composition of marine phytoplankton. Annu. Rev. Mar. Sci. 5, 191–215.

Twining, B.S., Nodder, S.D., King, A.L., Hutchins, D.A., LeCleir, G.R., DeBruyn, J.M., et al., 2014. Differential remineralization of major and trace elements in sinking diatoms. Limnol. Oceanogr. 59, 689–704.

Vance, D., Little, S.H., de Souza, G.F., Khatiwala, S., Lohan, M.C., Middag, R., 2017. Silicon and zinc biogeochemical cycles coupled through the Southern Ocean. Nat. Geosci. 10, 202–206. https://doi.org/10.1038/ngeo2890.

Varela, D.E., Willers, V., Crawford, D.W., 2011. Effect of zinc availability on growth, morphology, and nutrient incorporation in a coastal and an oceanic diatom. J. Phycol. 47, 302–312.

Wyatt, N.J., Milne, A., Woodward, A.M.E., Rees, A.P., Browning, T.J., Bouman, H.A., Worsfold, P.J., Lohan, M.C., 2014. Biogeochemical cycling of dissolved zinc along the GEOTRACES South Atlantic transect GA10 at 40°S. Glob. Biogeochem. Cycles 28. https://doi.org/10.1002/2013GB004637.

Zhao, Y., Vance, D., Abouchami, W., de Baar, H.J.W., 2014. Biogeochemical cycling of zinc and its isotopes in the Southern Ocean. Geochim. Cosmochim. Acta 125, 653–672.